Robust Myelin Quantitative Imaging from Multi-echo T2 MRI Using Edge Preserving Spatial Priors

Xiaobo Shen[1], Thanh D. Nguyen[2], Susan A. Gauthier[2], and Ashish Raj[2]

[1] Department of Computer Science, Cornell University, Ithaca, NY
xs83@cornell.edu
[2] Department of Radiology, Weill Cornell Medical College, New York, NY
{tdn2001,sag2015,asr2004}@med.cornell.edu

Abstract. Demyelinating diseases such as multiple sclerosis cause changes in the brain white matter microstructure. Multi-exponential T2 relaxometry is a powerful technology for detecting these changes by generating a myelin water fraction (MWF) map. However, conventional approaches are subject to noise and spatial in-consistence. We proposed a novel approach by imposing spatial consistency and smoothness constraints. We first introduce a two-Gaussian model to approximate the T2 distribution. Then an expectation-maximization framework is introduced with an edge-preserving prior incorporated. Three-dimensional multi-echo MRI data sets were collected from three patients and three healthy volunteers. MWF maps ob-tained using the conventional, Spatially Regularized Non-negative Least Squares (srNNLS) algorithm as well as the proposed algorithm are compared. The proposed method provides MWF maps with improved depiction of brain structures and significantly lower coefficients of variance in various brain regions.

Keywords: T2 relaxometry, myelin water fraction, edge-preserving priors.

1 Introduction

Multi-echo T2 relaxometry is a MR imaging technique in which a series of T2-weighted images are obtained at different echo times. It is a powerful tool to detect tissue damages in various demyelinating diseases such as multiple sclerosis (MS) [1]. By fitting a multi-exponential decay curve to this data, it is possible to deduce the T2 distribution of various water compartments in brain tissues to analyze their contributions separately. In particular, this analysis can provide numerical evaluation of the relative contribution of the myelin water compartment, represented as myelin water fraction (MWF), which can be used to assess the healthiness of white matter (WM).

Conventional approach [2] to extracting MWF can be easily impacted by small amounts of measurement noise and image artifacts. Consequently, diagnostically acceptable quality can only come from greatly increasing the number of sampled echoes [3] or much higher SNR, but these cause clinically unfeasible scan time. To reduce scan time, several authors have proposed alternative methods based on the gradient echo data acquisition with multi-compartmental steady-state signal [4], [5].

K. Mori et al. (Eds.): MICCAI 2013, Part I, LNCS 8149, pp. 622–630, 2013.

Recently, spatial smoothing constraints were proposed to improve the stability of the solution [6], [7]; however, these methods nevertheless rely on the single-voxel approach with a strong reliance on a pre-computed reference image. We have recently developed a spatial constrained algorithm parameterizing the T2 distribution into 2 Gaussian peaks and a long T2 component. Not only does this approach reduce the number of unknowns into 8 per voxel, it also allows for efficient, iterative conjugate gradient type algorithms. However, global, convex constraints are subject to tissue boundary blurring.

In this paper, we extend the spatial constrained approach to incorporate an edge-preserving prior (EPP) proposed by Raj et al [8] into a expectation-maximization (EM) style framework. The maximization (energy minimization) part applies EPP to the height parameters of two Gaussian peaks with a Quadratic Pseudo-Binary Optimization (QPBO) algorithm[9]. The expectation part updates other parameters with a nonlinear least square algorithm. We demonstrate the improvements by comparing the proposed method with the conventional and Spatially Regularized Non-negative Least Squares Algorithm (srNNLS method) [6] using visual and numerical assessments on simulated data and in vivo data.

2 Theory

2.1 Conventional T2 Relaxometry Analysis

At each voxel, given MR signals y measured at echo times TE_k (k = 1,..., K), a set i = 1,...,N of discrete sub-components are hypothesized to exist, each producing an exponentially decaying signal $\alpha_i \exp(-TE_k/T_2(i))$ with a known T2 constant of $T_2(i)$ and an unknown volume fraction of α_i . Assuming a slow exchange regime [10], the signal equation can be written as following:

$$y(TE_k) = \sum_{i=1}^{N} \alpha_i \exp\left(-\frac{TE_k}{T_2(i)}\right) + \varepsilon \quad (1)$$

or equivalently, $\mathbf{y} = \mathbf{A}\mathbf{x} + \boldsymbol{\varepsilon}$, with $\mathbf{A}_{ki} = \exp(-TE_k/T_2(i))$. Vector $\mathbf{y}$ is a collection of data y_k acquired at echo time TE_k, $\mathbf{x}$ is a vector of the unknown α_i, and $\boldsymbol{\varepsilon}$ denotes the noise vector. This linear system is typically under-determined (N>K) and ill-posed, making it hard to solve for $\mathbf{x}$ [2], [11]. Voxel-wise Tikhonov regularization [12] was proposed to partially overcome this problem with a non-negative least square (NNLS) algorithm. Unfortunately, the robustness requires extremely high SNR and more sampled echoes [13].

2.2 Multi-voxel Iterative Expectation-Maximization (EM) style Algorithm

Our proposed method encodes an EPP that T2 characteristics of the water compartments change smoothly within coherent brain regions but change abruptly across region boundaries. We first model the T2 distribution as a sum of two Gaussian distributions (one for the fast relaxing myelin water pool (T2~20 ms) and the other for the slower intra/extracellular water pool (T2~80 ms)), whose parameters (mean

location, height and variance) are unknown. We also add a very long relaxing cerebrospinal fluid (CSF) pool with unknown T2 and strength. Thus in the i-th voxel v_i we have the following set of unknowns: $\theta(v_i) = \{\alpha_1(i), m_1(i), \sigma_1(i), \alpha_2(i), m_2(i), \sigma_2(i), h_{CSF}(i), m_{CSF}(i)\}$, where α, m and σ stand for the height, mean and variance of the Gaussian peak, and $\boldsymbol{h_{CSF}}$ and $\boldsymbol{m_{CSF}}$ are the height and location for the CSF signal. So the T2 distribution at that voxel is: $\boldsymbol{x}_i(\tau) = \boldsymbol{\mathcal{G}}(\theta(v_i), \tau) = \alpha_1(i)\mathcal{N}\big(\tau|\, m_1(i), \sigma_1(i)\big) + \alpha_2(i)\mathcal{N}\big(\tau|\, m_2(i), \sigma_2(i)\big) + h_{CSF}(i)\,\delta(\tau - m_{CSF}(i)$, where each Gaussian is denoted as $\mathcal{N}(\cdot)$, δ denotes the delta function, and the T2 distribution is over the variable τ which is a set of sampled T2. By keeping τ fixed for all voxels, we have $\boldsymbol{x}_i = \boldsymbol{\mathcal{G}}\big(\theta(v_i)\big)$. Secondly, we collect multi-voxel parameters into a vector $\bar{\boldsymbol{\theta}} = \{\theta(v_i), i = 1, \ldots, N_v\}$, and map the Gaussian parameters to the resulting vectors of T2 distributions for all voxels by $\bar{\mathbf{x}} = \boldsymbol{\mathcal{G}}(\bar{\boldsymbol{\theta}})$. Single voxel quantity **y** is also collected into a multi-voxel vector $\bar{\mathbf{y}}$. The expanded matrix is similarly defined as A_{exp}. We then use the nonlinear least square (NLS) algorithm to minimize the non-convex function:

$$\hat{\boldsymbol{\theta}} = \arg\min_{\bar{\boldsymbol{\theta}}} \left\|\bar{\mathbf{y}} - A_{exp}\boldsymbol{\mathcal{G}}(\bar{\boldsymbol{\theta}})\right\|^2 + \mu_N \left\|D_N\bar{\boldsymbol{\theta}}\right\|^2 \tag{2}$$

Where D_N is a diagonal matrix whose diagonal elements are the normalization factors corresponding to each element in $\theta(v_i)$, and μ_N is the overall regularization scalar. We also define the residual data cost vector $\bar{\mathbf{C}} = \{c(v_i), i = 1, \ldots, N_v\}$ for all voxels, and it can be simply calculated by substituting $\bar{\boldsymbol{\theta}}$ into the following equation:

$$\bar{\mathbf{C}} = \left\|\bar{\mathbf{y}} - A_{exp}\boldsymbol{\mathcal{G}}(\bar{\boldsymbol{\theta}})\right\|^2 + \mu_N \left\|D_N\bar{\boldsymbol{\theta}}\right\|^2 \tag{3}$$

Thirdly, we can obtain the optimized $\widehat{\boldsymbol{\alpha}_1}$ and $\widehat{\boldsymbol{\alpha}_2}$ from $\hat{\boldsymbol{\theta}}$ in Eq. 2. The optimized $\hat{\mathbf{C}}$ is obtained by substituting $\hat{\boldsymbol{\theta}}$ into Eq. 3. $\hat{\mathbf{C}}$, $\widehat{\boldsymbol{\alpha}_1}$ and $\widehat{\boldsymbol{\alpha}_2}$ provide the prior information which can be used for constructing the costs of single-voxel (unary) and pairwise terms for QPBO. Towards the construction, the value ranges of $\widehat{\boldsymbol{\alpha}_1}$ and $\widehat{\boldsymbol{\alpha}_2}$ are first discretized into **n** levels respectively, and each level is for a candidate α-expansion move [8]. The discretization is carried out non-uniformly based on the frequency of values in $\widehat{\boldsymbol{\alpha}_1}$ or $\widehat{\boldsymbol{\alpha}_2}$. After discretization, we have **n** levels $l_1 = \{min(\widehat{\boldsymbol{\alpha}_1}), \ldots, \max(\widehat{\boldsymbol{\alpha}_1})\}$ for $\widehat{\boldsymbol{\alpha}_1}$. For each potential α-expansion for $\widehat{\boldsymbol{\alpha}_1}$ where $\alpha \in l_1$, the cost $\bar{\mathbf{C}}_{\mathbf{exp}}$ can be calculated by replacing α_1 of all voxels in $\hat{\boldsymbol{\theta}}$ with the

Table 1. Cost definition, where N_p is the number of pixels at slice $\boldsymbol{s}$, and $\hat{\mathbf{C}}_s$ and $\bar{\mathbf{C}}_{\mathbf{exp}_s}$ denote the subset for only slice $\boldsymbol{s}$. Binary label $\mathrm{b_i} = 1$ indicates an expansion move to α at pixel i. $\widehat{\boldsymbol{\alpha}_{1_s}}$ denotes the subset for only slice $\boldsymbol{s}$, and Nei is a set of all non-duplicated neighbor pixel index pairs on slice $\boldsymbol{s}$.

Unary or pairwise term	Cost
$\mathrm{B_1(b_i)}\ \ i \in \{1, \ldots, N_p\}, \mathrm{b_i} = 0$	$\hat{\mathbf{C}}_s(i)$
$\mathrm{B_1(b_i)}\ \ \mathrm{b_i} = 1$	$\bar{\mathbf{C}}_{\mathbf{exp}_s}(i)$
$\mathrm{B_2(b_i, b_j)}\ \ (i,j) \in Nei, i \neq j, \mathrm{b_i} = 0, \mathrm{b_j} = 0$	$\lvert\widehat{\boldsymbol{\alpha}_{1_s}}(i) - \widehat{\boldsymbol{\alpha}_{1_s}}(j)\rvert$
$\mathrm{B_2(b_i, b_j)}\ \ \mathrm{b_i} = 0, \mathrm{b_j} = 1$	$\lvert\widehat{\boldsymbol{\alpha}_{1_s}}(i) - \alpha\rvert$
$\mathrm{B_2(b_i, b_j)}\ \ \mathrm{b_i} = 1, \mathrm{b_j} = 0$	$\lvert\alpha - \widehat{\boldsymbol{\alpha}_{1_s}}(j)\rvert$
$\mathrm{B_2(b_i, b_j)}\ \ \mathrm{b_i} = 1, \mathrm{b_j} = 1$	0

scalar α and then substituting the modified $\hat{\boldsymbol{\theta}}$ into Eq. 3. Since the slice separation of MR data is much larger than slice resolution, we applied QPBO algorithm slice by slice. The unary and pairwise costs for each slice s are defined in Table 1.

Based on Table 1, we minimize the following function for slice s by QPBO (M part):

$$E_s = \arg\min_{b_i,b_j} \sum_{i=1}^{N} B_1(b_i) + \mu_S \sum_{(i,j)\in Nei} B_2(b_i, b_j) \qquad for\ \forall i, \qquad b_i \in \{0,1\} \tag{4}$$

where μ_S is the spatial regularization scalar for all pairwise cost terms. If the resulted binary label $b_i = 1$, we update $\widehat{\boldsymbol{\alpha}_{\mathbf{1}_s}}(i) = \alpha$ and $\hat{\mathbf{C}}_s(i) = \bar{\mathbf{C}}_{\mathbf{exp}_s}(i)$, and we do this for all slices. The expansion moves for $\widehat{\boldsymbol{\alpha}_2}$ are achieved in the same manner. After finishing all expansion moves for $\widehat{\boldsymbol{\alpha}_1}$ and $\widehat{\boldsymbol{\alpha}_2}$, we update the remaining 6 parameters in $\hat{\boldsymbol{\theta}}$ by using a NLS algorithm (E part). This can be simply done by minimizing Eq. 4 with fixed α_1 and α_2 terms. Typically over 2-4 iterations, we can obtain stable results.

3 Methods

3.1 Data

(1) Real data. One healthy volunteer at 1.5T using the conventional 3D multi-echo spin echo (MESE) sequence, two healthy volunteers and three MS patients at 3T using a 3D T2prep spiral sequence were obtained on a commercial MR imager (GE HDxt, GE Healthcare, Waukesha, WI). The imaging parameters were as follows: 3D MESE: axial FOV = 30 cm, matrix size = 256x128, partial phase FOV factor = 0.6, slice thickness = 5 mm, number of slices = 12, TR = 2500 ms, echo spacing = 5 ms, number of TEs = 32, scan time = 38 min; 3D T2prep spiral: axial FOV = 24-30 cm, matrix size = 192x192, slice thickness = 5 mm, number of slices = 32, TR = 2500 ms, flip angle = 10°, number of TEs = 15-26, scan time = 10-26 min. The SNR of a data set was calculated according to [14]. The average SNR of the three healtjy data sets was 339±150. The average SNR of three MS subjects was 456±46.

(2) Simulated data. Synthetic image data based on Montreal Neurological Institute (MNI) brain template were generated at SNR level varying from 100 to 1000. We first set the volume fraction weighted by the probabilities of WM and GM from the MNI template. Then Gaussian noise is artificially added to generate different SNR levels.

3.2 Algorithm Implementation and Parameter Optimization

Lsqnonlin function in MATLAB (R2011b) was used to solve Eq. 2. QPBO package (Version 1.3) was used. The whole program runs on a PC (Intel core 2 Duo processor at 2.2GHz, 4GB memory). Sparse matrices were adopted for storing voxel indexing used by lsqnonlin and pairwise voxel neighborhood.

We adopted a supervised trial and error method to find the optimal μ_N and μ_S with different choices of μ_N or μ_S varying logarithmically from 10^{-2} to 10^{-4}.

We assess the spatial quality of the MWF map and the numerical residual of NLS fitting for each choice and we select the value that represents the best compromise between data fidelity and visual quality. The processing duration was collected by running proposed algorithm with optimal parameter sets. The diagonal values of matrix D_N were determined empirically based on our knowledge to the general T2 distribution of brain voxels. For instance, we assign higher values (higher penalty) to its elements corresponding to myelin water pool because this pool accounts for smaller percentage of total signal.

3.3 Evaluation criteria

MWF was calculated as the ratio of signal integral from the myelin water signal to the integral of the total signal. For simulated data, mean square errors (MSE) of the algorithm resulted MWF maps with the true MWF maps were calculated at various SNR.

For MR data, Two quantitative criteria were used to compare the proposed algorithm to the conventional algorithm: 1) the spatial variation of MWF map within brain structures, as measured by the coefficient of variance (COV); 2) the ability to distinguish myelin-rich WM from lesion, as measured by the p-value (two-tailed two-sample t-tests) of MWF differences observed between selected normal WM ROI and selected lesion ROI in each patient subject. P-values of less than 0.05 were considered statistically significant.

4 Results

Figure 1 compares MSE of MWF maps for brain simulated data, demonstrating the improved accuracy obtained with the proposed method compared to the srNNLS method and the conventional method, particularly at low SNR.

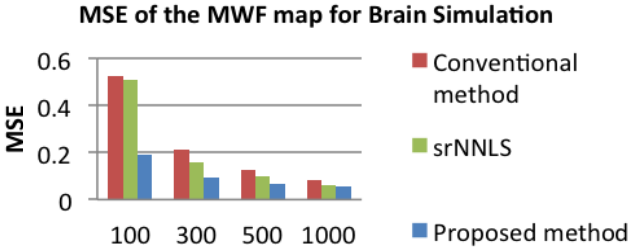

Fig. 1. Comparisons of mean square error (MSE) of the MWF map for Brain Simulation among three methods at SNR ∈ {100, 300, 500, 1000}

For real data, Figure 2 shows MWF maps obtained from three healthy subjects. The proposed approach provides higher spatial coherence and better depiction of the WM structures. Bottom row of Figure 2 shows anatomical T2-prep spiral images

wherein regions of low signal intensity correspond to WM tissues with high myelin content (except CSF regions which also appear dark). Table 2 summarizes mean COVs calculated within various regions for the MWF maps of the three subjects.

Table 2. Comparisons of Mean Coefficient of Variance (COV) of MWF in various ROIs

	Mean Coefficient of Variance (COV) of MWF maps		
	Conventional	srNNLS	Proposed
WM	0.8358	0.7638	0.1287
GM	1.1479	0.9873	0.2023
Genu of corpus callosum	0.4505	0.3702	0.0850
Splenium of corpus callosum	0.4781	0.4003	0.1084
Internal capsule	0.2775	0.2476	0.0629

Three patient sets were used for assessing performance of differentiating normal WM and lesion. The average P-values for Conventional, srNNLS and proposed method are 0.086, 0.069 and 0.0018. Figure 3 is the selected visual results for lesion differentiation.

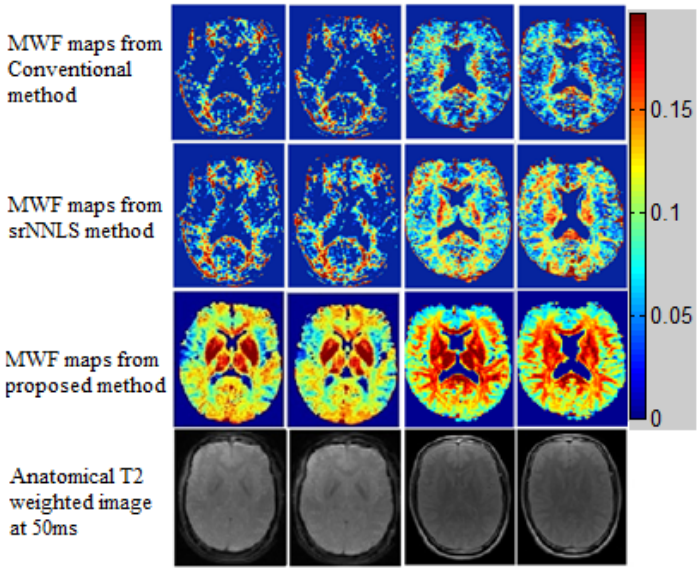

Fig. 2. Visual results for real healthy brain data (from left to right are 2 pairs of MWF slices from 2 real data sets). The left pair is from the isotropic 3D T2prep spiral data acquired at 3T and the right pair is from anisotropic 3D MESE data acquired at 1.5T.

We can see that the proposed method differentiated lesions better than the other two, while the conventional and srNNLS methods resulted in almost identical results.

The processing durations for 9 slices of size 192x192 pixels were approximately 4 hours, 6 hours and 2.7 hours with conventional, srNNLS method and proposed methods.

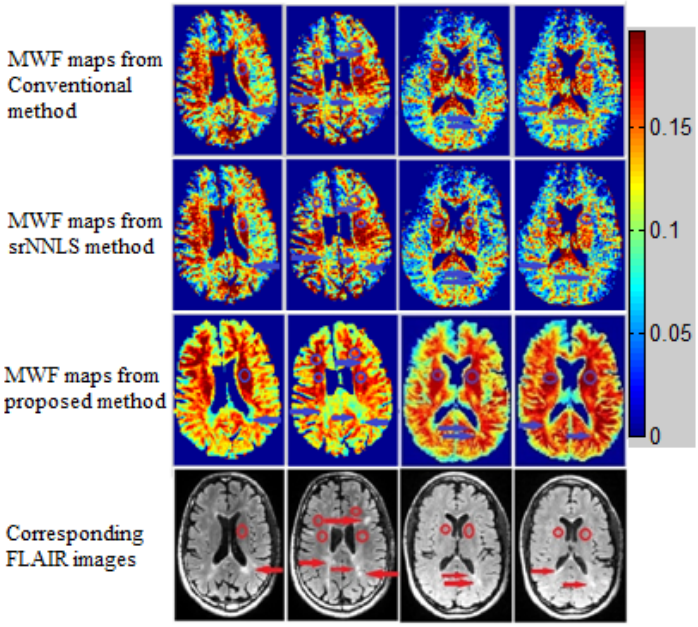

Fig. 3. Visual results for real patient brain data (from left to right are 2 pairs of MWF slices from 2 patient data sets). The red arrows in FLAIR images point to the lesions, and the blue arrows in MWF maps point to the corresponding areas. The red circles in FLAIR images represent the selected normal WM ROIs for calculating p-value, and the blue circles in MWFs is the corresponding areas

5 Discussion

This study demonstrated that the MWF maps obtained with the proposed method are less noise and better spatial consistency. The coverage within the white matter is significantly larger, with clear depiction of even fine and juxtacortical WM structures. The corpus callosum is faithfully depicted, and so are frontal projection fibers. Numerically, for simulated data, the MSEs from the proposed method at various SNRs are significantly lower. For real data, the mean COV of the proposed method demonstrated improved local smoothness at various ROIs. The improvment of the proposed algorithm for distinguishing WM and lesions is substantiated by p-values.

Compared with Kumar et al [14], the MWF maps generated from our algorithm have similar appearance but better visual quality in terms of visual smoothness and delineation of different brain structures. With our proposed method, the MWFs for genu of corpus callosum, splenium of corpus callosum and internal capsules are 17.1±1.8%, 15.5±2.0% and 18.1±1.0% separately over three healthy subjects. The corresponding values reported in [14] are 16.7±1.8%, 14.6±3.1% and 14.2±1.5%, and the corresponding values reported in [15] are 10.2±0.2%, 14.4±0.2% and 17.2±0.2%. The COV values were slightly higher than that Oh et al reported in [16] and lower than that Kumar et al reported in [14]. The above deviations may be due to the use of

different modality data, limited number of subjects and the various sizes of the selected ROIs. Compared with mcDESPOT [4], the proposed method is able to infer the T2 distribution rather 2 pure water pools.

The primary clinical goal for this work is to produce whole brain MWF maps for patients with MS. The improved robustness of our algorithm against noise effect may therefore benefit recently developed rapid 3D spiral T2 relaxometry sequences for whole brain coverage, in which SNR was traded for acquisition time.

References

[1] Laule, C., Vavasour, I.M., Moore, G.R.W., Oger, J., Li, D.K.B., Paty, D.W., MacKay, A.L.: Water content and myelin water fraction in multiple sclerosis. A T2 relaxation study. Journal of Neurology 251(3), 284–293 (2004)

[2] Whittall, K.P., MacKay, A.L.: Quantitative interpretation of NMR relaxation data. Journal of Magnetic Resonance 84(1), 134–152 (1969)

[3] Haacke, E.M., Brown, R.W., Thompson, M.R., Venkatesan, R.: Magnetic Resonance Imaging: Physical Principles and Sequence Design, p. 1008. Wiley-Liss (1999)

[4] Deoni, S.C.L., Rutt, B.K., Arun, T., Pierpaoli, C., Jones, D.K.: Gleaning multicomponent T1 and T2 information from steady-state imaging data. Magnetic Resonance in Medicine: Official Journal of the Society of Magnetic Resonance in Medicine/Society of Magnetic Resonance in Medicine 60(6), 1372–1387 (2008)

[5] Kolind, S.H., Deoni, S.C.: Rapid three-dimensional multicomponent relaxation imaging of the cervical spinal cord. Magnetic Resonance in Medicine: Official Journal of the Society of Magnetic Resonance in Medicine / Society of Magnetic Resonance in Medicine 65(2), 551–556 (2011)

[6] Hwang, D., Du, Y.P.: Improved myelin water quantification using spatially regularized non-negative least squares algorithm. Journal of Magnetic Resonance Imaging: JMRI 30(1), 203–208 (2009)

[7] Bjarnason, T.A., McCreary, C.R., Dunn, J.F., Mitchell, J.R.: Quantitative T2 analysis: the effects of noise, regularization, and multivoxel approaches. Magnetic Resonance in Medicine: Official Journal of the Society of Magnetic Resonance in Medicine/Society of Magnetic Resonance in Medicine 63(1), 212–217 (2010)

[8] Raj, A., Singh, G., Zabih, R., Kressler, B., Wang, Y., Schuff, N., Weiner, M.: Bayesian parallel imaging with edge-preserving priors. Magnetic Resonance in Medicine: Official Journal of the Society of Magnetic Resonance in Medicine/Society of Magnetic Resonance in Medicine 57(1), 8–21 (2007)

[9] Boros, E., Hammer, P.L.: Pseudo-Boolean optimization. Discrete Applied Mathematics 123(1-3), 155–225 (2002)

[10] Lancaster, J.L., Andrews, T., Hardies, L.J., Dodd, S., Fox, P.T.: Three-pool model of white matter. Journal of Magnetic Resonance Imaging: JMRI 17(1), 1–10 (2003)

[11] Haacke, E.M., Brown, R.W., Thompson, M.R., Venkatesan, R.: Magnetic Resonance Imaging: Physical Principles and Sequence Design, p. 1008. Wiley-Liss (1999)

[12] Tychonoff, A.N., Arsenin, V.Y.: Solution of Ill-posed Problems. Winston, New York (1977)

[13] Graham, S.J., Stanchev, P.L., Bronskill, M.J.: Criteria for analysis of multicomponent tissue T2 relaxation data. Magnetic Resonance in Medicine: Official Journal of the Society of Magnetic Resonance in Medicine/Society of Magnetic Resonance in Medicine 35(3), 370–378 (1996)

[14] Kumar, D., Nguyen, T.D., Gauthier, S.A., Raj, A.: Bayesian algorithm using spatial priors for multiexponential T(2) relaxometry from multiecho spin echo MRI. Magnetic Resonance in Medicine: Official Journal of the Society of Magnetic Resonance in Medicine/Society of Magnetic Resonance in Medicine (January 2012)

[15] Meyers, S.M., Laule, C., Vavasour, I.M., Kolind, S.H., Mädler, B., Tam, R., Traboulsee, A.L., Lee, J., Li, D.K.B., MacKay, A.L.: Reproducibility of myelin water fraction analysis: a comparison of region of interest and voxel-based analysis methods. Magnetic Resonance Imaging 27(8), 1096–1103 (2009)

[16] Oh, J., Han, E.T., Pelletier, D., Nelson, S.J.: Measurement of in vivo multi-component T2 relaxation times for brain tissue using multi-slice T2 prep at 1.5 and 3 T. Magnetic Resonance Imaging 24(1), 33–43 (2006)